



Hydrodynamically enhanced electrochemical mass transfer on the surface of an electrically conductive droplet

A. Kharicha¹ · E. Karimi-Sibaki¹ · A. Vakhrushev¹ · M. Wu² · A. Ludwig² · J. Bohacek³

Received: 13 October 2020 / Accepted: 31 March 2021
© The Author(s) 2021

Abstract

A fully coupled model is proposed to investigate the influence of flow on electrochemical mass transfer at the interface between the electrolyte and an electrically conductive droplet. The electric current flows through the droplet, and consequently the droplet acts as both anode and cathode. Computations of flow, concentration of reactant, and electric current density fields were carried out. Various droplet sizes (0.5, 2, 4 mm) under different flow regimes considering Reynolds number ($Re = 0.2, 2, 20, 40$ and 80) were investigated. An iterative numerical method is proposed to determine the concentration of reactant and electric current density at droplet-electrolyte interface considering the reaction kinetics (Butler-Volmer) formula and the diffusion-advection of the reactant through the hydrodynamic boundary layer around the droplet. With the increase of Reynolds number, the amount of electric current density which flows through the droplet increases. It is found that the mass transfer at droplet-electrolyte interface is controlled by reaction kinetics for the small droplet (0.5 mm). However, the diffusion of the reactant governs the efficiency of mass transfer with the increase of the droplet size (2 and 4 mm). With the increase of Reynolds number, the anodic area on the surface of droplet is enlarged.

1 Introduction

Many metallurgical processes make the use of strong electric currents through electrolytes. The aim is either heating/melting the metal or promoting electrochemical mass transfer at electrolyte-metal interface [1]. As an example, heating is used to melt large metallic electrodes in the electrosag remelting process [2]. In this process, very high AC or DC electric current in the range between 40 to 200 kA.m^{-2} are passed through the electrolyte as known as slag. Thanks to Joule heating, the temperature in the slag raises to 2300 K that results in the melting of the immersed metallic electrode and formation of droplets of

various sizes (0.1–10 mm). Smaller amount electric current density ($<15 \text{ kA.m}^{-2}$) are used in the production of liquid aluminum in Hall-Heroult process where small droplets ($<<1 \text{ mm}$) are generated as soon as electric current flows through the cryolite-aluminum interface [3]. Those droplets are generated as a consequence of a very violent phenomenon associated with the metal pad and short circuiting noise [3, 4]. In copper refining processes with the presence of copper droplets, a peculiar phenomenon was observed in which small copper droplets behave as insulating while larger ones are fully conductive [5, 6]. Apparently, suspension of metallic droplets in electrolytes is a common phenomenon in electrometallurgy.

Generally, the aforementioned processes involve a strong convection within the electrolyte due to the interaction between the flow and electric current through Magnetohydrodynamics (MHD). Thus, it is impossible to avoid the generation of relatively small metallic droplets at the liquid metal-electrolyte interface [7].

The role of such droplets, isolated or in the form of clouds, on the performance of those processes is a major scientific and technical question. The presence of a cloud of droplets (conducting or not) will deflect the electric current that in turn promotes new kinds of interfacial instabilities. Furthermore, the electrochemical mass transfer at the droplet-electrolyte interface plays a decisive role on the overall refining process of the metal.

✉ A. Kharicha
Abdellah.kharicha@unileoben.ac.at

¹ Christian-Doppler Laboratory for Metallurgical Applications of Magnetohydrodynamics, Montanuniversitaet of Leoben, Franz-Josef-Str. 18, A-8700 Leoben, Austria

² Chair of Simulation and Modeling of Metallurgical Processes, Montanuniversitaet of Leoben, Franz-Josef-Str. 18, A-8700 Leoben, Austria

³ Heat Transfer and Fluid Flow Laboratory, Faculty of Mechanical Engineering, Brno University of Technology, Technicka 2896/2, 616 69 Brno, Czech Republic

In fluid dynamical systems, the flow field and concentration field are always interdependent. As such, the variation in the intensity of flow (more precisely hydrodynamic boundary layer) impacts the concentration field (more precisely concentration boundary layer) that in turn determines the mass transfer at interfaces.

Far too little attention has been paid in the literature to suspension of metallic droplets in electrolytes although it is a common phenomenon in electrometallurgy. The present paper aims in studying the influence of the flow of electrolyte on the ability of a metallic droplet to conduct a DC Current, and consequently to determine the mass transfer at droplet-electrolyte interface. Customarily, the flow is characterized using Reynolds number that is dependent on the size of the droplet and the relative velocity between the droplet and the surrounding fluid. Herein, different droplets sizes and electrolyte velocities, corresponding to Reynolds numbers up to 80 are investigated.

2 Modeling

The well-established Finite Volume Method (FVM) is applied for numerical simulation of flow, concentration of cupric ion (Cu^{2+}), and electric fields. The commercial CFD software, ANSYS FLUENT v.14.5, was utilized to carry out simulations. Several User-defined functions (UDF) are implemented for special modeling equations e.g. to model Butler-Volmer reaction kinetics, Poisson-Boltzmann distribution, etc. The configuration of the system is schematically illustrated in Fig. 1. A 2D axisymmetric computational domain is considered. In the present study, the system is composed of a copper droplet and the copper sulfate-sulfuric acid electrolyte for which kinetic and hydrodynamic properties (e.g. exchange current density, viscosity, etc.) are well-known [8]. All symbols are listed in “Nomenclature”. In the bulk of electrolyte, the concentration field (c_∞), the velocity field (u_∞), and the electric field (E_∞) are prescribed. Note that, the droplet acts as both cathode and anode. Thus, the cathodic/anodic area on the surface of droplet must be computed that in turn depends on the intensity of the flow and the droplet size (more precisely Reynolds (Re) number). Cupric ion is injected into the electrolyte at the anodic part of droplet, whereas it is consumed at the cathodic part.

2.1 Governing eqs

A summary of all governing equations and corresponding boundary conditions are listed in Table 1.

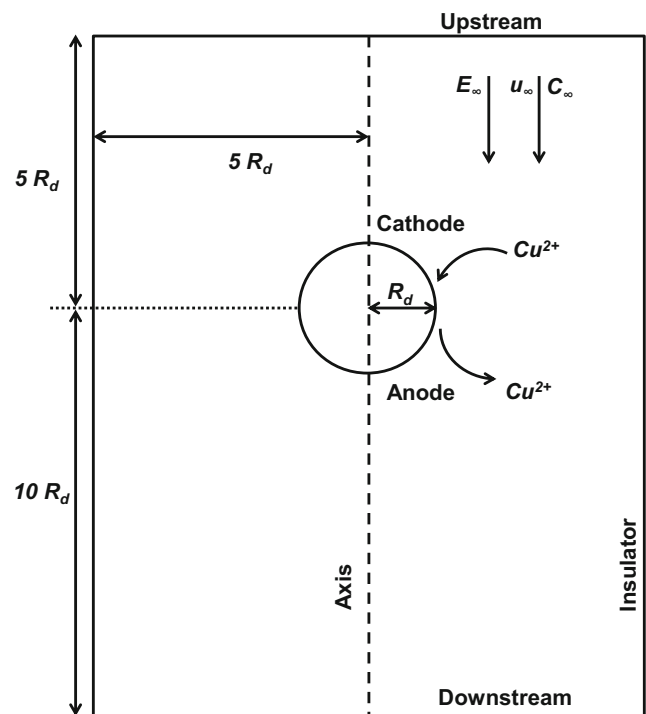


Fig. 1 Configuration of the computational domain and boundaries are schematically illustrated. The droplet acts as both the anode and cathode where cupric ion (Cu^{2+}) participates in Faradaic reactions

2.1.1 Flow field

As described in Table 1, The Navier-Stokes continuity, Eq. (1), and momentum, Eq. (2), equations are used to calculate the velocity field. The fluid (electrolyte) is regarded as Newtonian and incompressible under isothermal condition. The velocity field in the bulk of electrolyte is specified to u_∞ . The characteristic of the hydrodynamic boundary layer which develops around the droplets depends on u_∞ and the droplet size through Reynolds number. The boundary conditions related to flow are summarized in Table 1.

2.1.2 Concentration field of Cu^{2+}

Following the conventional approach to neglect the migration flux in the presence of the excess of supporting electrolyte, the diffusion-advection equation is solved to obtain the concentration field (c) of cupric ion [9] as described in Table 1 using Eq. (3). Accordingly, the boundary conditions to determine the concentration field are described in Table 1. The boundary condition at droplet surface is completely dependent on the electric current density that will be further elucidated in the following section.

2.1.3 Electric current density field

The conservation of electric current density (j) is obtained through Laplace equation, Eq. (4) in Table 1, where electric

Table 1 Governing equations and corresponding boundary conditions of flow, concentration of reactant, and electric current density fields

Flow field

$$\frac{\partial \rho}{\partial t} + \nabla \cdot (\rho \vec{u}) = 0 \quad (1)$$

$$\frac{\partial (\rho \vec{u})}{\partial t} + \nabla \cdot (\rho \vec{u} \vec{u}) = -\nabla p + \nabla \cdot [\mu (\nabla \vec{u} + \vec{u}^T)] + \rho \vec{g} \quad (2)$$

Concentration field of Cu^{2+}

$$\frac{\partial c}{\partial t} = -\nabla \cdot [\vec{u} c - D_{\text{Cu}^{2+}} \nabla c] \quad (3)$$

Electric current density

$$\nabla \cdot (-\sigma \nabla \varphi) = 0 \quad (4)$$

Boundary conditions

$$\text{Upstream: } u = u_\infty, -\frac{\partial \varphi}{\partial n} = E_\infty, c = c_\infty$$

$$\text{Downstream: Pressure-outlet, } \varphi = 0, \frac{\partial c}{\partial n} = 0$$

$$\text{Insulator: Free-slip, } \frac{\partial \varphi}{\partial n} = 0, \frac{\partial c}{\partial n} = 0$$

Droplet surface: No-slip,

$$j = j_0 \left(\frac{c}{c_\infty} \right) \left[e^{\left[\frac{\alpha z_{\text{Cu}^{2+}} F \eta}{RT} \right]} - e^{\left[\frac{(1-\alpha) z_{\text{Cu}^{2+}} F \eta}{RT} \right]} \right] \quad (5)$$

$$D_{\text{Cu}^{2+}} \frac{\partial c}{\partial n} = \frac{j}{z_{\text{Cu}^{2+}} F} \quad (\text{Cathodic part}) \quad (6)$$

$$c = c_\infty e^{\left[\frac{z_{\text{Cu}^{2+}} F \eta}{RT} \right]} \quad (\text{Anodic part}) \quad (7)$$

current density is calculated using Ohm's law ($\vec{j} = -\sigma \nabla \varphi$). Boundary conditions to calculate the electric current density are also described in Table 1.

Special care must be taken to assign boundary conditions at droplet surface where electric current density and concentration of Cu^{2+} are fully coupled. The flux of electric potential (\approx electric current density) is assigned at droplet surface where the calculated concentration of Cu^{2+} is set as boundary condition for Eq. (3). In modeling point of view, the droplet surface is a conjugate wall where the influence of the formation of electric double layer (EDL) at electrolyte-metal interface is implicitly modeled. Here the electrochemical kinetic at the interface is taken into account, whereas charge accumulation is neglected. The jump in electric potential at the interface (η) as a conjugate wall appears in Butler-Volmer formula (Eq. (5)). Of note, the sign of j is positive at anodic part of droplet. In contrast, it is negative at the cathodic part of droplet. The sign enables us to distinguish the anodic and cathodic part of the droplet throughout calculations. At the cathodic part, the contribution of diffusion in the potential drop across EDL is taken into account through Eq. (6). On the other hand, the electric current density is obtained using Eq. (7) at the anodic part of droplet where the concentration is assigned based on Poisson-Boltzmann.

An iterative procedure is executed to calculate j and c as follows: Firstly, the sign of j is used to determine the cathodic/anodic area on the droplet. Secondly, j is calculated through Butler-Volmer formula using Eq. (5). Thirdly, the calculated j is used to obtain c at the interface for cathodic part through Eq. (6) or for the anodic part through Eq. (7). Finally, the newly calculated value of c is inserted back to Butler-Volmer formula, Eq. (5), to re-calculate j . The procedure continues until the convergence criterion (e.g. here residuals below 10^{-6}) is satisfied.

2.2 Model verification

To best of our knowledge, there exists no direct experimental measurements or an analytical solution for the system (conductive droplet in an electrolyte) modeled in this paper. The ability of our developed code to model electrochemical systems has been successfully validated numerous times [10, 11]. Additionally, we examined our developed code as the infrastructure of the presented model in this manuscript against classical electrochemical systems such as flow between planes as known as channel flow cells or cathodic rotating disc electrode (RDE). Herein, we noticed that mass transfer phenomenon in the presented study involving a conductive droplet inside an electrolyte behaves in accordance with classical electrochemical systems. Based on our modeling results, we will show that the system reaches to a limiting current density [9].

As an example, herein, we briefly present our investigation on the behavior of cathodic rotating disc electrode (RDE) system to demonstrate our verification procedure of the presented model. Marathe and Newman [12] conducted a series of experiment to study transport phenomena in an electrochemical cell involving the cathodic rotating disc electrode (RDE). For the simulations, we used the identical geometry, material (an electrolyte made of 0.1 M copper sulfate and 0.1 M sulfuric acid), and operational parameters [12]. The cathodic RDE spins with the rotation rate of 300 rpm. As shown in Fig. 2, a comparison is made between our simulation results and their experimental measurements. The electric current distribution along the surface of the rotating cathode is assessed. Two distinct applied voltages (0.2 V and 0.4 V) are examined. Apparently, the amount of the average electric current density increases with the enlargement of the applied voltage. Satisfactory agreements between the aforementioned methods are achieved.

2.3 Other settings

A total number of 40,000 mesh elements are initially used to generate the grid within the computational domain. However, the grid is adapted (refined) in the vicinity of droplet electrolyte interface during calculations to ensure capturing hydrodynamics and concentration boundary layers. The third-order

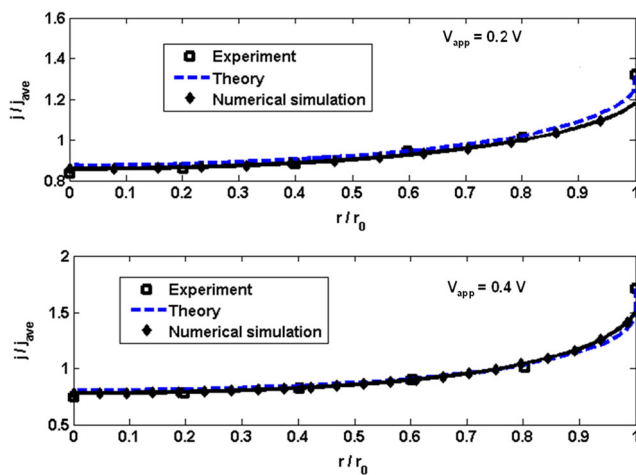


Fig. 2 A comparison is made among the theoretical current distribution obtained from Newman's theory [12], experimental measurements [12], and our numerical results considering two different applied voltages: firstly, $V_{app}=0.2$ V for which $j_{ave}=125$ A. m^{-2} , and secondly, $V_{app}=0.4$ V for which $j_{ave}=320$ A. m^{-2}

MUSCL scheme is utilized for spatial discretization of governing equations that enables us to accurately handle variable grid sizes [13, 14]. The temporal numerical discretization is according to first-order implicit method [13, 14]. Transient calculations were made to achieve steady-state solutions. Therefore, the equations were solved by means of the pseudo-transient computation technique in which the transient terms (temporal derivatives) were retained [13]. Capturing the transient behavior of the system is not the objective as the steady state problem is embedded in a space-time setting. Thus, the temporal accuracy is sacrificed in favor of rapid

Table 2 Parameters used in our calculations. The material properties are extracted from Ref. [8]

Parameter	
R [J K^{-1} mol $^{-1}$]	8.314546
g [m s^{-2}]	9.81
T [K]	293
F [A s mol $^{-1}$]	96,485
E_{∞} [V m^{-1}]	35
σ_e [S m^{-1}]	5.1
σ_d [S m^{-1}]	1×10^7
ρ [kg m^{-3}]	1030
μ [kg m^{-1} s $^{-1}$]	0.00103
α	0.5
j_0 [A m^{-2}]	10
c_{∞} [mol m^{-3}]	10
	0.61×10^{-9}
$D_{Cu^{2+}}$ [m 2 s $^{-1}$]	
n	2
$z_{Cu^{2+}}$	+2

convergence to the steady state. This technique is effective for non-linear problems when the initial solution is far from the final steady state [10, 15].

The steady state results were further evaluated. The material properties of electrolyte and droplet as well as operating conditions are listed in Table 2. The properties are extracted from Ref. [8]. Several droplet sizes (0.5, 2, 4 mm) under different flow regimes ($Re=0.2, 2, 20, 40$ and 80) were examined.

3 Results and discussions

Computed field structures including velocity, concentration of cupric ion (Cu^{2+}), and electric current density fields for the droplet with the size of 2 mm at different Reynolds number are shown in Fig. 3. A recirculating zone as known as vortex ring is observed close to the rear stagnation point of the droplet at $Re=80$ as shown in Fig. 3(a). Taneda [16] pointed out that the vortex ring starts to develop at $Re=24$. Experimental analysis and measurements indicated that the vortex ring expands as Reynolds number increases [16]. The diameter of vortex ring reaches to that of the droplet at about $Re=130$. At this point, the flow close to the stagnation point becomes unstable and consequently the vortex ring begins to oscillate [16]. As anticipated, the flow remarkably influences the distribution of concentration of Cu^{2+} . The concentration boundary layer diminishes as Reynolds number increases as illustrated in Fig. 3(b). Thereby, the amount of electric current density which flows through the droplet is significantly impacted as shown in Fig. 3(c). In the absence of the vortex ring, a region of low concentration of Cu^{2+} is observed in the front part of the droplet where the droplet acts as a cathode. In contrast, a region enriched in Cu^{2+} is noticed in the rear part of the droplet where the droplet acts as an anode. The enriched region forms a tail in the rear part of droplet indicating that the injected Cu^{2+} from the anodic part of droplet is carried by the flow. Furthermore, the thickness of the tail decreases as Reynolds number increases. The presence of the vortex ring remarkably influences the concentration field of Cu^{2+} around the droplet as shown in Fig. 3(b) for $Re=80$. The aforementioned tail disappears that leads to the formation of a very narrow region enriched in Cu^{2+} adjacent to the droplet. Apparently, the amount of electric current density which flows through the droplet increases as the Reynolds number increases that is illustrated in Fig. 3(c).

An extensive series of simulation were performed to explore the effect of droplet size on the electrochemical behavior of the system considering different values of Reynolds number i.e. $Re=0.2, 2, 20, 40$ and 80 . The amount of electric current density is plotted versus the position on the surface of droplet that is demonstrated using the angle coordinate. Furthermore, each plot is labeled

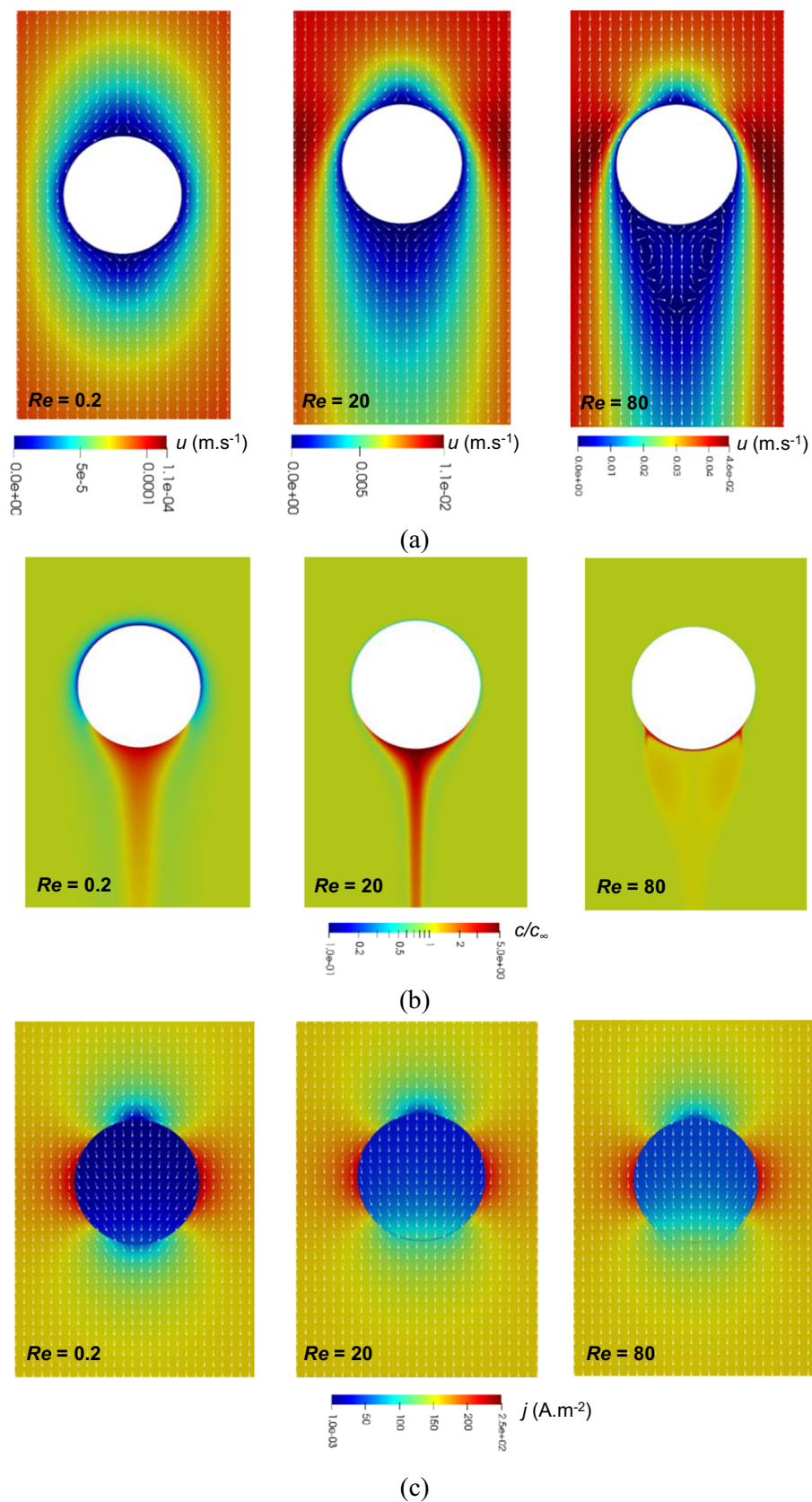


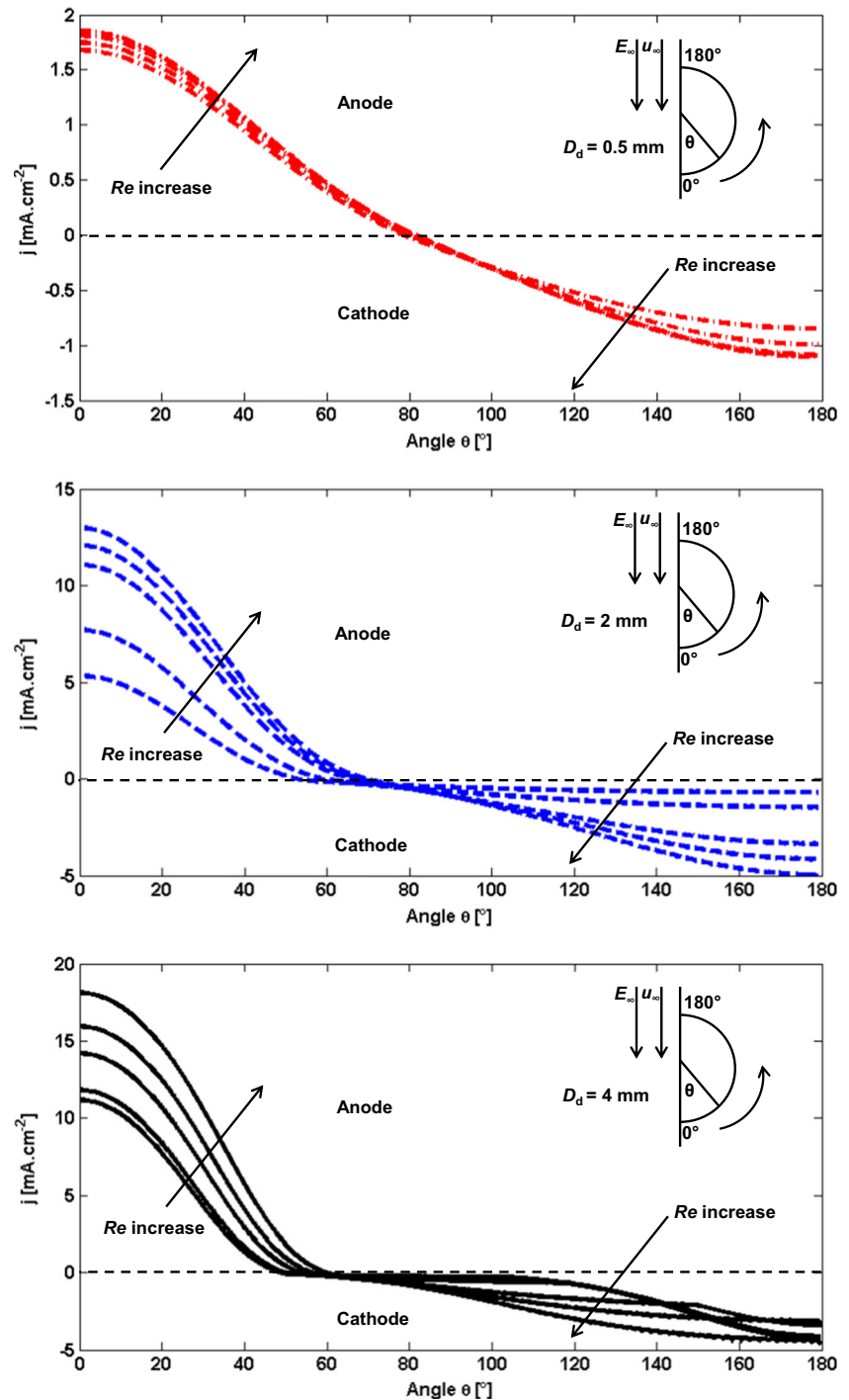
Fig. 3 Field structures are illustrated at different Reynolds number ($Re = 0.2, 20$, and 80) for the droplet with the size of 2 mm. Each contour is labeled using the magnitude of Reynolds number. **a** Velocity field; **b**

normalized concentration field in logarithmic scale; **c** Electric current density field. Equisized vectors are used in (a) and (c) to indicate the direction

according to the size of droplet as shown in Fig. 4. The small droplet with the size of 0.5 mm is almost insensitive to the variation of the intensity of the flow. The electric current density on the surface of droplet slightly increases as Reynolds number increases. Additionally, the surface area of the anode is nearly equal to that of the cathode as the sign of electric current density is switched from positive (anode) to negative (cathode) at the angle of ca. 90°. This implies

that mass transfer is dominantly governed by the reaction kinetics for the small (0.5 mm) droplet. With the increase of droplet size (2 and 4 mm), the amount of surface electric current density is notably influenced by the flow. The area of anode as well as the amount of electric current density which flows through the droplet increases as Reynolds number increases. This implies that the mass transfer is controlled by the mechanism of diffusion for large droplets (2

Fig. 4 The electric current density is plotted along the surface of droplet. Each plot is labeled using the droplet size. Directions of bulk electric field and bulk flow field are indicated

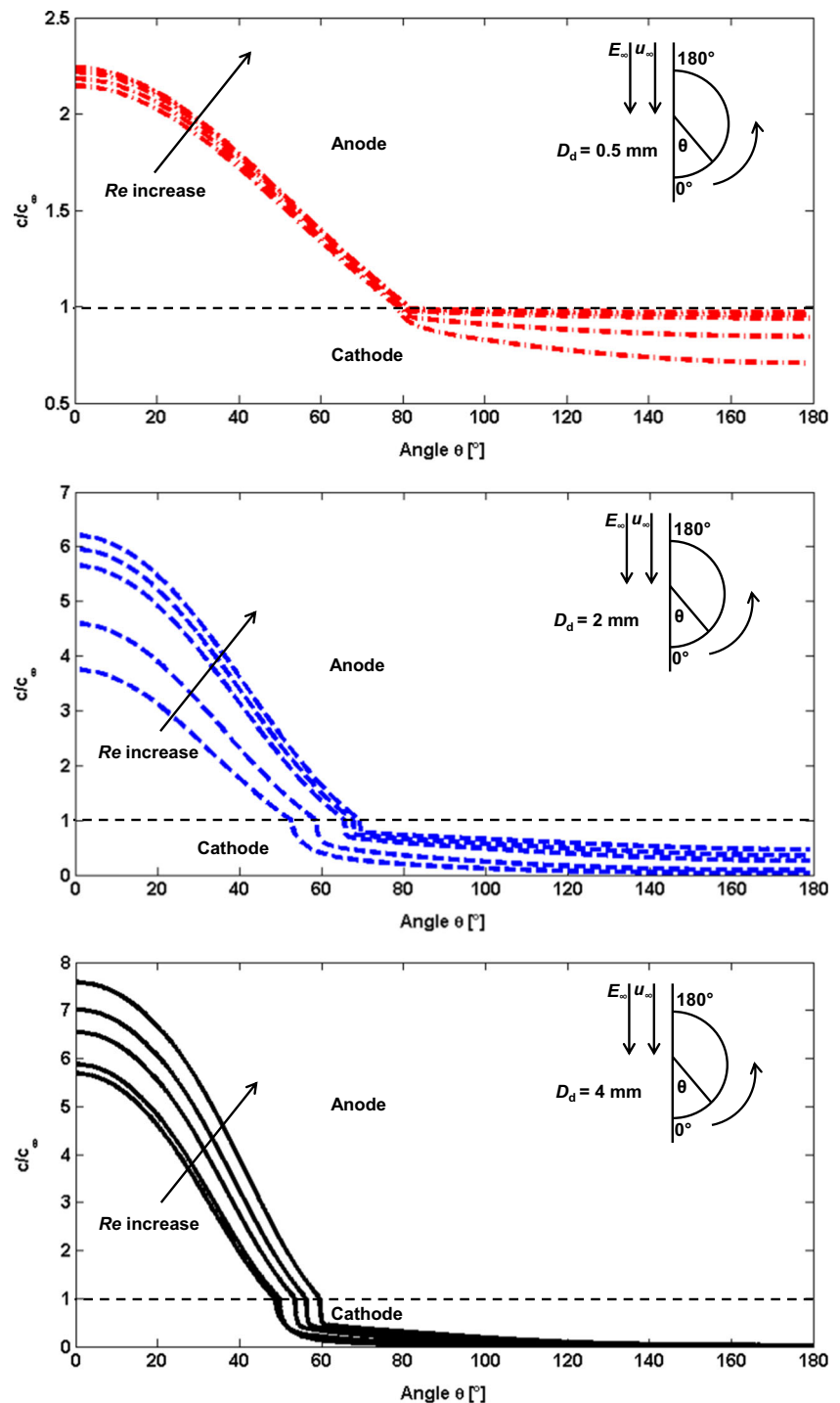


and 4 mm). Furthermore, the area of cathode/anode on the surface of droplet is dependent on the droplet size regardless of Reynolds number. The ratio of anodic area to cathodic area of the surface of droplet decreases as the droplet size increases at constant Reynolds number.

The distribution of the concentration of Cu^{2+} on the surface of droplet considering different droplet size is illustrated in Fig. 5. The concentration of Cu^{2+} and electric

current density are correlated through Eq. (5)–(7). As such, the variation in concentration of Cu^{2+} on the surface of droplet follows the same trend as the electric current density. The front part of the droplet acts as the cathode. The limiting current density is acquired on a portion of the cathodic region for the large droplet with the size of 4 mm. In this case, the magnitude of concentration of Cu^{2+} becomes nearly zero above the angle of ca. 140° .

Fig. 5 The concentration of Cu^{2+} is plotted along the surface of droplet. Each plot is labeled using the droplet size. Directions of bulk electric field and bulk flow field are indicated



The relationship between Reynolds number and the total amount of electric current which flows through the droplet for different droplet size is shown in Fig. 6. An exponential relationship is noticed among the aforementioned parameters regardless of the droplet size. This implies that there exists a maximum allowable (limiting) current although the total amount of electric current through the droplet increases as the flow intensifies.

4 Summary

The electrochemical mass transfer at a droplet-electrolyte interface is investigated by the help of computational fluid dynamics tools. The transport phenomena including flow,

concentration of reactant (here cupric ion), and electric current density fields are computed. The concentration of the reactant and electric potential are fully coupled so that the interplay between the reaction kinetics at the droplet-electrolyte interface (Butler-Volmer formula) and the diffusion-advection of reactant through the hydrodynamic boundary layer around the droplet is taken into account. The condition of the presences of excess of supporting electrolyte is assumed to ignore the migration transport of the reactant. The droplet acts as both the cathode and anode. Thus, the cathodic/anodic area on the surface of droplet is computed that in turn depends on the intensity of the flow and the droplet size (more precisely Reynolds (Re) number). Numerous droplet sizes (0.5, 2, 4 mm) under different flow regimes ($Re = 0.2, 2, 20, 40$ and 80) were evaluated. Expectedly, the amount of electric current (\sim mass transfer) which flows through the droplet increases as the flow intensifies. We found that the mass transfer at droplet-electrolyte interface is controlled by reaction kinetics for the small droplet (0.5 mm), whereas the role of diffusion becomes more potent with the increase of the droplet size (2 and 4 mm). Furthermore, the anodic area on the surface of droplet grows as Reynolds number increases.

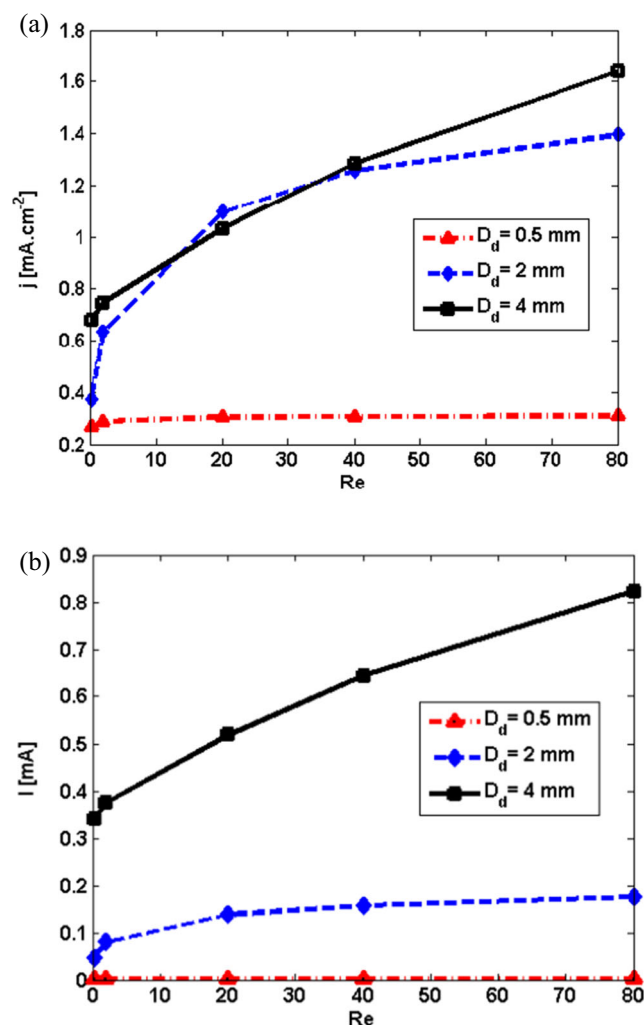


Fig. 6 The relationship among the total amount of electric current density which flows through the droplet and Reynolds number considering different droplet size (0.5, 2, and 4 mm) is shown. **a** Electric current density; **b** Electric current

Nomenclature Cu^{2+} , Cupric ion; c , Concentration of cupric ion / mol m^{-3} ; c_∞ , Bulk concentration of cupric ion / mol m^{-3} ; $D_{Cu^{2+}}$, Diffusion coefficient of cupric ion / $\text{m}^2 \text{s}^{-1}$; E_∞ , Bulk electric field / V m^{-1} ; F , Faraday constant / A s mol^{-1} ; g , Gravity constant / m s^{-2} ; j , Electric current density / A m^{-2} ; j_0 , Exchange current density / A m^{-2} ; j_{ave} , Average current density on RDE cathode / A m^{-2} ; n , Number of exchanged electrons; p , Pressure / Pa ; R , Universal gas constant / $\text{J K}^{-1} \text{mol}^{-1}$; t , Time / s ; T , Temperature / K ; u , Velocity vector / m s^{-1} ; V_{app} , Applied voltage of RDE / V ; r , Distance along the surface of RDE cathode / m ; r_0 , Radius of RDE cathode / m ; Re , Reynolds number; $z_{Cu^{2+}}$, Charge number of cupric ion; α , Charge transfer coefficient in Butler-Volmer (BV) formula; ρ , Density / kg m^{-3} ; μ , Dynamic viscosity / $\text{kg m}^{-1} \text{s}^{-1}$; φ , Electric potential / V ; η , Activation overpotential / V ; σ_e , Electrical conductivity of electrolyte / S m^{-1} ; σ_d , Electrical conductivity of droplet / S m^{-1} ; $\frac{\partial}{\partial n}$, Derivative along the outward-drawn normal to the boundary surface / m^{-1}

Acknowledgements The authors acknowledge financial support from the Austrian Federal Ministry of Economy, Family and Youth and the National Foundation for Research, Technology and Development within the framework of the Christian-Doppler Laboratory for Metallurgical Applications of Magnetohydrodynamics.

Author's contribution **A. Kharicha**: Conceptualization, Methodology, Supervision, Writing - original draft.

E. Karimi-Sibaki: Conceptualization, Methodology, Software, Visualization, Writing - original draft.

A. Vakhrushev: Visualization.

M. Wu: Supervision.

A. Ludwig: Supervision, Administration.

J. Bohacek: Methodology.

Funding Open access funding provided by Montanuniversität Leoben.

Open Access This article is licensed under a Creative Commons Attribution 4.0 International License, which permits use, sharing, adaptation, distribution and reproduction in any medium or format, as long as you give appropriate credit to the original author(s) and the source, provide a link to the Creative Commons licence, and indicate if changes were made. The images or other third party material in this article are included in the article's Creative Commons licence, unless indicated otherwise in a credit line to the material. If material is not included in the article's Creative Commons licence and your intended use is not permitted by statutory regulation or exceeds the permitted use, you will need to obtain permission directly from the copyright holder. To view a copy of this licence, visit <http://creativecommons.org/licenses/by/4.0/>.

References

1. Reynolds QG (2015) Mathematical and computational modelling of MHD effects in en-trained droplets of slag and metal, the fourteenth international ferroalloys congress, Kiev, Ukraine
2. Chaulet J, Kharicha A, Charmond S, Dussoubs B, Hans S, Wu M, Ludwig A, Jardy A (2020) A 2D multiphase model of drop behavior during Electrosag Remelting. *Metals* 10:490
3. Bojarevics V and Romero MV Long waves instability of liquid metal-electrolyte interface in aluminium electrolysis cells: a generalization of Sele's criterion. *Eur J Mech, B/Fluids* 13:33
4. Bojarevics V (1998) Nonlinear waves with electromagnetic interaction in aluminium electrolysis cells. In: Branover H, Unger Y (eds.) *Progress in Fluid Flow Research: Turbulence and Applied MHD*. Progress in Astronautics and Aeronautics (182). American Institute of Aeronautics and Astronautics, Reston, pp 833–848. <https://doi.org/10.2514/4.866531>
5. Warczok A, Riveros G (2007) Slag cleaning in crossed electric and magnetic fields. *Miner Eng* 20:34
6. Warczok A, Riveros G (2002) Electromagnetic buoyancy force of copper inclusion in a liquid slag. *Proc. ConametSAM-Simp. Mater.*, Santiago, Chile
7. Coursol P, Dufour G, Côté J, Chartrand P, MacKay P (2012) Application of thermodynamic models for better understanding and optimizing the hall-Heroult process. *JOM* 64:1326
8. Georgiadou M (2003) Modeling current density distribution in electrochemical systems. *Electrochim Acta* 48:4089
9. Newman J, Thomas-Alyea KE (2004) *Electrochemical systems*. John Wiley & Sons, New Jersey
10. Karimi-Sibaki E, Kharicha A, Wu M, Ludwig A, Bohacek J (2018) Confrontation of the ohmic approach with the ionic transport approach for modeling the electrical behavior of an electrolyte. *Ionics* 24:2157
11. Karimi-Sibaki E, Kharicha A, Wu M, Ludwig A, Bohacek J (2018) Contribution of an electro-vortex flow to primary, secondary, and tertiary electric current distribution in an electrolyte. *J Electrochem Soc* 165:E604–E615
12. Marathe V, Newman J (1969) Current distribution on a rotating disk electrode. *J Electrochem Soc* 116:1704
13. Versteeg H, Malalasekera W (2007) *An introduction to computational fluid dynamics: the finite volume method*. Pearson Education Limited, Essex
14. Van Leer B (1979) Toward the ultimate conservative difference scheme. V. a second-order sequel to Godunov's method. *J Comput Phys* 32:101
15. Coffey TS, Kelley CT, Keyes DE (2003) Pseudotransient continuation and differential-algebraic equations. *SIAM J Sci Comput* 25: 553
16. Taneda S (1956) Experimental investigation of the wake behind a sphere at low Reynolds numbers. *J Phys Soc Jpn* 11:1104–1108

Publisher's note Springer Nature remains neutral with regard to jurisdictional claims in published maps and institutional affiliations.